Heterogeneous Catalysis

DOI: 10.1002/anie.200503068

On the Role of Oxygen Defects in the Catalytic Performance of Zinc Oxide**

Sebastian Polarz, Jennifer Strunk, Vladislav Ischenko, Maurits W. E. van den Berg, Olaf Hinrichsen,* Martin Muhler, and Matthias Driess*

Metal oxides are highly important as components in heterogeneous catalysts.[1] It is also well established that as the building blocks of nanoscaled materials get smaller, surfaces become increasingly important in determining their properties.[2] Very early on, researchers found that catalytic activity is only indirectly related to the surface area;[3] in fact it depends on the density of active sites.[4] Although solid-state defects have been proposed to be the active sites in heterogeneous catalysis,[5] active centers have rarely been conclusively identified and the rational design of catalysts is still out of reach.

Processes in heterogeneous catalysis associated with the production of energy-storage molecules, for example, methanol as a storage molecule for hydrogen,[6,7] is presently of great interest. Low-pressure production of methanol is conducted industrially with catalysts containing Cu and ZnO as the active phases and alumina as the support.[7,8] Composites (Cu + ZnO), however, exhibit higher activities than that expected based on the performance of the single components. This was attributed to a strong metal–support interaction (SMSI) effect.[9] Nevertheless, the active sites in Cu/ZnO and even in the pure ZnO have not yet been identified experimentally.

Some important information concerning pure ZnO catalysts is already available: Generally, the catalytic activity of ZnO does not increase linearly with the increasing BET surface area.[10] It was concluded that the catalytic formation of methanol over ZnO is a structure-sensitive reaction requiring the presence of polar ZnO facets.[10] According to the most recent models of the methanol-synthesis reaction on the polar ZnO(000$\bar{1}$) surface,[11] oxygen vacancies formed on this surface of ZnO crystals serve as the active sites (Scheme 1).[12] However, there has been no definite experimental proof for this assumption.

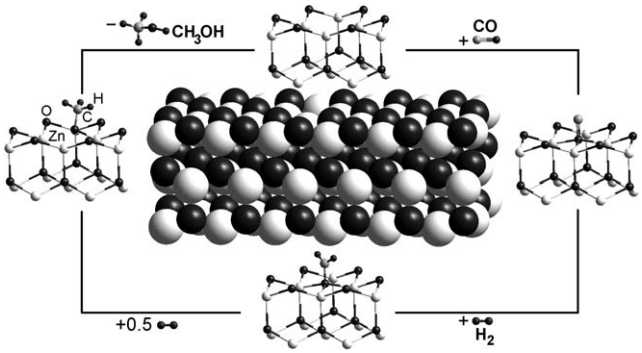

Scheme 1. Model for the activity of ZnO in the hydrogenation of CO. The space-filling model shows the (000$\bar{1}$) surface with one oxygen vacancy. The ball-and-stick models show the chemisorption of CO at the oxygen vacancy. More detailed information is given in Ref. [11].

We report here on the preparation of nanocrystalline ZnO materials containing different amounts of oxygen vacancies and on the catalytic performance of this model system. Our results indicate that oxygen vacancies are of fundamental importance for explaining the catalytic activity of pure ZnO in methanol synthesis.

The presence of oxygen vacancies in ZnO has been known for some time,[13] and a number of methods are suitable for the preparation of surface-rich and nanoscaled ZnO.[14] Still, to our knowledge no one has studied nanocrystalline ZnO with a varying degree of oxygen deficiencies and the effect on catalytic properties. One reason for this may be the thermodynamic instability of such vacancies at "normal" oxygen partial pressures.[15] One theoretical study implies that ZnO with oxygen defects is only metastable. Therefore, these materials may be accessible only by kinetically controlled bottom-up routes. We recently identified an organometallic precursor system from which ZnO can be prepared at temperatures as low as 150 °C.[16–19] These molecular precursors are characterized by a central Zn_4O_4 heterocubane cluster and thus represent zinc oxide preorganized on the

[*] Dr. S. Polarz, Dr. V. Ischenko, Prof. Dr. M. Driess
Technical University Berlin, Institute of Chemistry
Strasse des 17. Juni 135, 10623 Berlin (Germany)
Fax: (+49) 234-321-4378
E-mail: sebastian.polarz@tu-berlin.de
Dipl.-Chem. J. Strunk, Dr. M. W. E. van den Berg, Prof. Dr. O. Hinrichsen, Prof. Dr. M. Muhler
Ruhr-Universität Bochum, Fakultät für Chemie
Universitätsstrasse 150, 44780 Bochum (Germany)
Fax: (+49) 30-314-297-32
E-mail: olaf@techem.ruhr-uni-bochum.de

[**] The authors gratefully acknowledge the Deutsche Forschungsgemeinschaft (DFG) for funding (Sonderforschungsbereich 558; Emmy Noether research group). We thank Dr. E. Bill and Prof. Dr. K. Wieghardt for the EPR measurements of our samples and for valuable discussions.

Supporting information for this article is available on the WWW under http://www.angewandte.org or from the author.

molecular scale. In Figure 1a the methylisopropoxy derivative $[CH_3ZnOCH(CH_3)_2]_4$ is shown as an example.

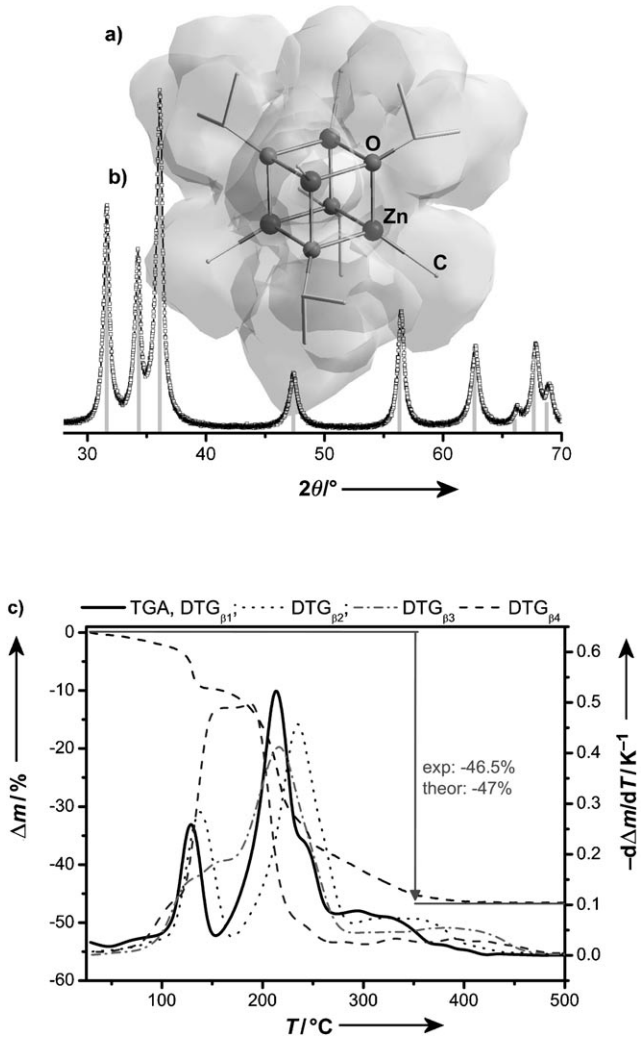

Figure 1. a) Molecular structure of the $[CH_3ZnOCH(CH_3)_2]_4$ highlighting the central Zn_4O_4 heterocubane motif; H atoms not shown. b) PXRD pattern of the material obtained from this precursor at $T_{end} = 350\,°C$ and a heating rate of $\beta_3 = 10\,K\,min^{-1}$, and the reference pattern of ZnO with hexagonal wurtzite structure (gray). c) TG curve for the thermolysis/oxidation of $[CH_3ZnOCH(CH_3)_2]_4$ in 80% N_2/20% O_2 and the first derivative of the TG trace (DTG) for the heating rates β_1–β_4.

The thermolysis of $[CH_3ZnOCH(CH_3)_2]_4$ in the presence of O_2 was studied by thermogravimetric analysis (TGA) at different heating rates β ranging from 1 $K\,min^{-1}$ to 30 $K\,min^{-1}$. It is evident that $[CH_3ZnOCH(CH_3)_2]_4$ is highly sensitive to kinetic factors in the decomposition process. At very low heating rates ($\beta_1 = 1\,K\,min^{-1}$) the thermolysis is characterized by two main mass-loss steps at $T = 128\,°C$ and 213 °C (Figure 1c). The remaining mass of 53.5% is in good agreement with the value expected for the quantitative transformation of the precursor to ZnO. At higher heating rates ($\beta_2 = 5\,K\,min^{-1}$ and $\beta_3 = 10\,K\,min^{-1}$, Figure 1b) the results can be explained by a broadening and superposition of the two DTG peaks (first derivative of the TGA data), but this is not possible for the highest heating rate ($\beta_4 = 30\,K\,min^{-1}$, Figure 1c). Only one broad step of mass loss is found centered at $T = 172\,°C$. The TGA results indicate that at higher heating rates formation of ZnO occurs under nonequilibrium conditions.

Interestingly, neither the chemical composition nor the particle size changes significantly with heating rate as proven by powder X-ray diffractometry (PXRD; not shown), elemental analysis, and IR spectroscopy. The IR spectra (see the Supporting Information) reveal that at 350 °C ZnO free of organic impurities could be obtained; only the features characteristic for the bulk ZnO reference sample are observed (ZnO stretching band at 440 cm^{-1}). Concerning this point, there is practically no difference between the samples heated at rates of 1 $K\,min^{-1}$ (β_2) and 30 $K\,min^{-1}$ (β_4). Therefore, we decided to heat our samples to $T_{end} = 350\,°C$ for their preparation. At this temperature one obtains pure, nanocrystalline ZnO with a mean particle diameter of roughly 13 nm as indicated by the PXRD pattern obtained for the sample with $\beta_3 = 10\,K\,min^{-1}$ (Figure 1b).[20] The purity of the obtained ZnO, in particular of its surface, was further confirmed by XPS measurements (see the Supporting Information).

Recently we were able to demonstrate by EPR spectroscopy that unpaired electrons are trapped at the sites of the oxygen vacancies.[18] The ZnO sample prepared from the *tert*-butoxy derivative $[CH_3ZnOCH(CH_3)_2]_4$ shows two EPR signals at *g*-values of around 1.96 and 2.0, the latter of which corresponds to the oxygen vacancies (Figure 2, top).

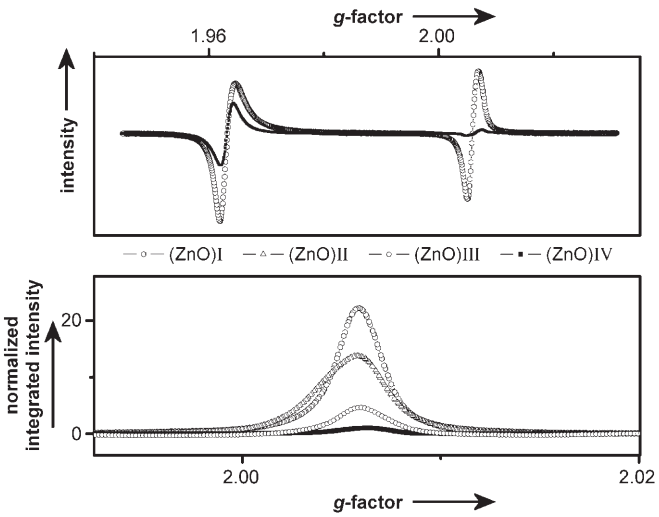

Figure 2. Top: EPR spectra of two ZnO samples prepared from $[CH_3ZnOC(CH_3)_3]_4$ at different heating rates of 5 $K\,min^{-1}$ (β_2, (ZnO)IV) and 30 $K\,min^{-1}$ (β_4, (ZnO)I). Bottom: The EPR data were normalized to the material with the lowest EPR signal ((ZnO)IV; see Table 1).

Details regarding the analysis of oxygen-deficient ZnO samples are beyond the scope of this paper, and the reader is referred to a separate publication.[18] An overview of the samples presented in the current study is given in Table 1. Initially, we believed that $[CH_3ZnOCH(CH_3)_2]_4$ is the ideal

Table 1: Overview over the samples used for the catalytic investigations.

Sample	Precursor	Conditions
(ZnO)I	$[CH_3ZnOC(CH_3)_3]_4$	$\beta_4 = 30\ K\,min^{-1}$
(ZnO)II	$[CH_3ZnOC(CH_3)_3]_4$	$\beta_3 = 10\ K\,min^{-1}$
(ZnO)III	$[CH_3ZnOCH(CH_3)_2]_4$	$\beta_2 = 5\ K\,min^{-1}$
(ZnO)IV	$[CH_3ZnOC(CH_3)_3]_4$	$\beta_2 = 5\ K\,min^{-1}$

precursor for obtaining oxygen-deficient ZnO owing to the possible elimination of acetone and the corresponding formation of zinc hydride as the reactive transient species (Scheme 2, see the Supporting Information).[17,19]

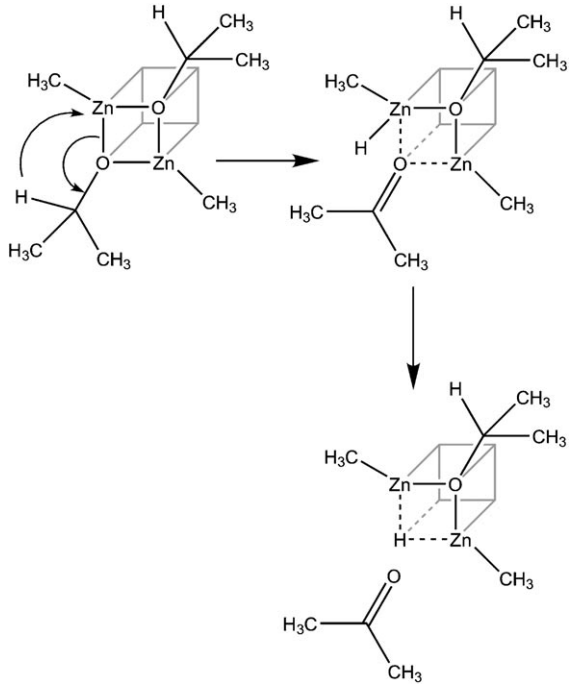

Scheme 2. Schematic representation of the loss of acetone from $[CH_3ZnOCH(CH_3)_2]_4$. For clarity only the front face of the "Zn_4O_4" cluster is shown. The products resulting from a β-hydride transfer must be regarded as intermediates in the formation of oxygen-deficient ZnO.

We tested our hypothesis whether the elimination of acetone is truly crucial for the formation of oxygen vacancies by comparison with a sample prepared from the *tert*-butoxy derivative $[CH_3ZnOC(CH_3)_3]_4$. Clearly, the elimination of an oxygen-containing leaving group from the *tert*-butoxy-substituted Zn_4O_4 core is rather unlikely because no β hydrogen atom is present. In fact, the intensity of the EPR signal corresponding to oxygen vacancies is smaller for a ZnO sample resulting from $[CH_3ZnOC(CH_3)_3]_4$ ((ZnO)IV) than that for a sample prepared from $[CH_3ZnOCH(CH_3)_2]_4$ ((ZnO)III; see Table 1 and Figure 2). The integrated intensity of the EPR signal corresponding to oxygen vacancies is five times higher for (ZnO)III than for (ZnO)IV, which indicates that the oxygen vacancy density is much lower for the latter sample. However, the effect was less pronounced than we had hoped.

Therefore, we raised the alternative hypothesis that more oxygen vacancies can be created if ZnO is prepared under enhanced nonequilibrium conditions. Figure 2a shows the results from EPR measurements of samples prepared from $[CH_3ZnOC(CH_3)_3]_4$ at $T_e = 350\,°C$ with different heating rates ((ZnO)IV: $\beta_2 = 5\ K\,min^{-1}$, (ZnO)I: $\beta_4 = 30\ K\,min^{-1}$). It can be seen that the EPR signal corresponding to oxygen vacancy sites at $g \approx 2.00$ is significantly higher for (ZnO)I.[18] The normalized, integrated intensity even 25 times greater (Figure 2b). Interestingly, $[CH_3ZnOCH(CH_3)_2]_4$ is less suitable for the formation of nanocrystalline ZnO with high oxygen-vacancy content, because at high heating rates we even observed the formation of elemental zinc (results not shown). Nevertheless, with $[CH_3ZnOC(CH_3)_3]_4$ as a precursor it is possible to obtain nanocrystalline ZnO samples with differing oxygen-vacancy content (Figure 2b).

Next, we tested the catalytic activity of the prepared samples for methanol synthesis (Figure 3) from using a

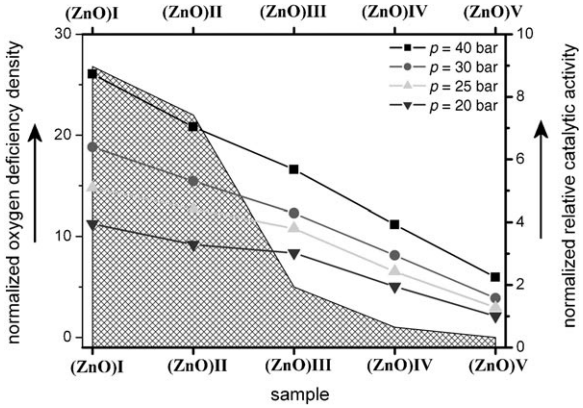

Figure 3. Correlation of the occurrence of oxygen vacancy sites (determined by EPR spectroscopy) to the normalized activity for CO hydrogenation at different pressures ($p = 20$–40 bar). The activities were normalized to the BET surface area of the respective ZnO powders and to the sample with lowest catalytic activity ((ZnO)V, a reference sample prepared by a conventional precipitation technique[10]).

feedgas mixture containing CO and H_2 (see the Experimental Section). Figure 3 indicates that a qualitative correlation exists between the catalytic activity and the amount of oxygen vacancies in the ZnO samples. While (ZnO)I has approximately over 25 times more oxygen vacancies than sample (ZnO)IV, its catalytic activity is only about four times higher. However, differences in scaling are expected since the catalytic activity is a surface property of the samples, while the EPR signal scales with the bulk volume of ZnO. Therefore, we conclude that the catalytic activity of ZnO does indeed depend on the amount of oxygen vacancies present.

Although there is a convincing correlation between the oxygen-deficiency content as determined by the EPR measurements, other factors like particle strain and the presence of more unstable crystal surfaces could also explain the higher catalytic performance of the kinetically produced ZnO samples.[18] If so, a similar trend in catalytic performance should also be observed for tests with CO_2 instead of CO. We reported earlier that CO_2 has a poisoning effect on pure ZnO

catalysts probably arising from the quenching of oxygen defect sites.[11] This poisoning effect is caused by the reaction of CO_2 with the oxygen vacancy accompanied by the release of CO. It is important to note that CO_2 can quench only oxygen defect sites on the surface and no other structural defects such as dislocations etc.[18] Therefore, only two scenarios are possible: 1) The ZnO samples introduced here could display unusual activity also under CO_2-rich conditions, indicating that factors other than oxygen vacancies are responsible for the catalytic performance. 2) The unusual features in catalytic properties could be quenched by CO_2, and the zinc oxide samples would be comparable to the reference samples in CO_2. In this case oxygen vacancies play a crucial role.

Consequently, we determined the catalytic activity of the our samples in an atmosphere containing CO_2 and compared the data to those recorded previously on conventional ZnO samples (Figure 4; for further details about the reference samples see reference [10]). The samples (ZnO)I–(ZnO)IV and the reference samples display almost identical behavior. This strongly suggests that oxygen vacancies are indeed responsible for the increased catalytic activity under a CO atmosphere.

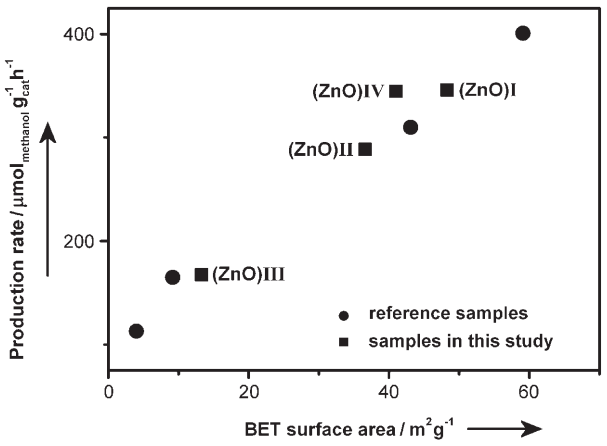

Figure 4. Catalytic performance of (ZnO)I–(ZnO)IV and of a reference sample[10] and in CO_2-containing synthesis gas (measurements at 30 bar).

In summary, samples with a set variation in oxygen-vacancy content can be prepared under kinetically controlled conditions by the low-temperature thermolysis of organometallic heterocubane Zn_4O_4 precursors. Catalytic investigations showed that oxygen vacancies in the ZnO lattice are very likely to represent the active sites in the hydrogenative conversion of CO to methanol.

Experimental Section

The heterocubane precursors and samples (ZnO)I–(ZnO)IV were prepared as reported in previous papers.[18,19] Sample (ZnO)V was prepared according to the literature.[10]

Catalytic measurements were performed in a previously described flow setup[21] with six gas lines: He (99.9999%), H_2 (99.9999%), 2% H_2/He (H_2: 99.9995%), 1% N_2O/He (N_2O: 99.9995%), 10% CO/He (CO: 99.9995%), and synthesis gas. Two different synthesis gas mixtures (purity ≥ 99.9995%) were used: 15% CO/H_2 and 6% CO/8% CO_2/64% H_2/He.[21] Fast online gas analysis was performed with a calibrated mass spectrometer (Balzers GAM422). In each test, 100 mg of the ZnO sample, previously pressed, crushed, and sieved to a particle size of 250–355 μm, was filled into a glass-lined stainless steel U-tube reactor. The catalyst bed was fixed by a glasswool plug on either side. The pretreatment of the samples comprised a heating procedure in 2% H_2/He (10 N mL min^{-1}, 5 K min^{-1}) from room temperature to 573 K and subsequently that temperature was maintained in dilute H_2 for 1 h. The reactor was flushed with He (10 N mL min^{-1}) for about 30 min without cooling, as a temperature of 573 K was also used for all catalytic activity tests. The temperature was measured and maintained throughout the test procedure by a thermocouple placed directly inside the catalyst bed. As the equilibrium yields in methanol synthesis are rather low at 573 K and atmospheric pressure, the reaction was carried out at 40, 30, 25, and 20 bar. At each pressure, conditions were maintained until steady state was reached.

Thermogravimetric analyses of the precursor were carried out with a thermogravimetric setup from Rubotherm. X-ray diffractograms were recorded with a Bruker AXS D8 Advance instrument using $Cu_{K\alpha}$ radiation ($\lambda = 1.5418$ Å) and a position-sensitive detector (PSD) diffractometer using $Cu_{K\alpha}$ radiation in the 2θ range from 25° to 85° with steps of 0.015°. Crystallite size and microstrain parameters were determined by full-profile LeBail fit of the experimental XRD pattern with subsequent decomposition of the reflection profile into Gaussian and Lorentzian parts, taking into account instrumental contribution to peak broadening. X-band EPR spectra were recorded with a Bruker Elexsys E500 EPR spectrometer with an ER077R magnet (75-mm pole cap distance), and an ER047 XG-T microwave bridge. The samples were irradiated with an Oriel high-pressure mercury lamp. The samples were loaded into quartz tubes and inserted into the microwave cavity. FT-IR spectra were recorded with a Bruker Vector 22 spectrometer (KBr pellets). The BET area was measured by static N_2 physisorption in the quartz U-tube of an Autosorb 1-C setup (Quantachrome). XPS spectra were recorded with a Scienta SES 2002 spectrometer using monochromated $Al_{K\alpha}$ radiation at 1486.6 eV. The X-ray source was operated at 14 kV and 55-mA emission current. Base pressure in the measurement chamber was less than 7×10^{-10} mbar. Survey spectra were recorded with a pass energy of 500 eV, whereas for the individual spectral lines 200 eV was used. The step size for the regions was 100 meV. Under these conditions, the Au $4f_{7/2}$ linewidth of a sputtered gold foil was 0.74 eV. All spectral lines were calibrated using the binding energy of the Zn $2p_{3/2}$ line at 1021.8 eV as a reference.

Received: August 29, 2005
Revised: February 13, 2006
Published online: March 28, 2006

Keywords: heterogeneous catalysis · methanol synthesis · oxygen vacancies · zinc oxide

[1] a) C. N. R. Rao, *Annu. Rev. Phys. Chem.* **1989**, *40*, 291; A. Fujimori, T. Mizokawa, *Curr. Opin. Solid State Mater. Sci.* **1997**, *2*, 18; b) Y. Tokura, *Curr. Opin. Solid State Mater. Sci.* **1998**, *3*, 175; c) R. J. Mortimer, *Chem. Soc. Rev.* **1997**, *26*, 147; d) P. Poizot, S. Laruelle, S. Grugeon, L. Dupont, J. M. Tarascon, *Nature* **2000**, *407*, 496.
[2] H. J. Freund, H. Kuhlenbeck, V. Staemmler, *Rep. Prog. Phys.* **1996**, *59*, 283.
[3] M. Boudart, *Cattech* **2001**, *5*, 81.
[4] H. S. Taylor, *Proc. R. Soc. London* **1925**, *108*, 105.

[5] J. M. Thomas, E. L. Evans, J. O. Williams, *Proc. R. Soc. London Ser. A* **1972**, *331*, 417.
[6] a) G. A. Olah, *Angew. Chem.* **2005**, *117*, 2692; *Angew. Chem. Int. Ed.* **2005**, *44*, 2636; b) K. C. Waugh, *Catal. Today* **1992**, *15*, 51; c) J. Agrell, B. Lindström, L. J. Pettersson, S. G. Järas in *Catalysis—Specialist Periodical Reports 16* (Ed.: J. J. Spivey), Royal Society of Chemistry, Cambridge, **2002**, p. 67.
[7] L. Lloyd, D. E. Ridler, M. V. Twigg in *Catalyst Handbook* (Ed.: M. V. Twigg), Wolfe, London, **1989**.
[8] a) G. C. Chinchen, K. C. Waugh, D. A. Whan, *Appl. Catal.* **1986**, *25*, 101; b) M. Kurtz, H. Wilmer, T. Genger, O. Hinrichsen, M. Muhler, *Catal. Lett.* **2003**, *86*, 77.
[9] a) H. Wilmer, O. Hinrichsen, *Catal. Lett.* **2002**, *82*, 117; b) M. Kurtz, N. Bauer, C. Buscher, H. Wilmer, O. Hinrichsen, R. Becker, S. Rabe, K. Merz, M. Driess, R. A. Fischer, M. Muhler, *Catal. Lett.* **2004**, *92*, 49; c) M. Kurtz, N. Bauer, H. Wilmer, O. Hinrichsen, M. Muhler, *Chem. Eng. Technol.* **2004**, *27*, 1146.
[10] H. Wilmer, M. Kurtz, K. V. Klementiev, O. P. Tkachenko, W. Grünert, O. Hinrichsen, A. Birkner, S. Rabe, K. Merz, M. Driess, C. Wöll, M. Muhler, *Phys. Chem. Chem. Phys.* **2003**, *5*, 4736.
[11] M. Kurtz, J. Strunk, O. Hinrichsen, M. Muhler, K. Fink, B. Meyer, C. Wöll, *Angew. Chem.* **2005**, *117*, 2850; *Angew. Chem. Int. Ed.* **2005**, *44*, 2790.
[12] a) J. C. Lavalley, J. Saussey, T. Rais, *J. Mol. Catal.* **1982**, *17*, 289; b) H. H. Kung, *Catal. Rev. Sci. Eng.* **1980**, *22*, 235; c) S. A. French, A. A. Sokol, S. T. Bromley, C. R. A. Catlow, S. C. Rogers, F. King, P. Sherwood, *Angew. Chem.* **2001**, *113*, 4569; *Angew. Chem. Int. Ed.* **2001**, *40*, 4437; d) S. A. French, A. A. Sokol, S. T. Bromley, C. R. A. Catlow, P. Sherwood, *Top. Catal.* **2003**, *24*, 161; e) H. Lüth, G. W. Rubloff, W. D. Grobman, *Solid State Commun.* **1976**, *18*, 1427; f) W. Göpel, *Surf. Sci.* **1977**, *62*, 165.
[13] a) A. Poppl, G. Volkel, *Phys. Status Solidi A* **1989**, *115*, 247; b) B. S. Chiou, M. C. Chung, *J. Electron. Mater.* **1991**, *20*, 885; c) V. A. Gercher, D. F. Cox, J. M. Themlin, *Surf. Sci.* **1994**, *306*, 279.
[14] a) S. J. Pearton, D. P. Norton, K. Ip, Y. W. Heo, T. Steiner, *J. Vac. Sci. Technol.* **2004**, *22*, 932; b) Z. L. Wang, *J. Phys. Condens. Matter* **2004**, *16*, R829; c) R. Viswanatha, S. Sapra, B. Satpati, P. V. Satyam, B. N. Dev, D. D. Sarma, *J. Mater. Chem.* **2004**, *14*, 661; d) G. Rodriguez-Gattorno, P. Santiago-Jacinto, L. Rendon-Vazquez, J. Nemeth, I. Dekany, D. Diaz, *J. Phys. Chem.* **2003**, *107*, 12597; e) Z. S. Hu, G. Oskam, P. C. Searson, *J. Coll. Interf. Sci.* **2003**, *263*, 454; f) M. Shim, P. Guyot-Sionnest, *J. Am. Chem. Soc.* **2001**, *123*, 11651; g) E. A. Meulenkamp, *J. Phys. Chem.* **1998**, *102*, 5566.
[15] B. Meyer, *Phys. Rev. B* **2004**, *69*.
[16] a) S. Polarz, F. Neues, M. Van den Berg, W. Grünert, L. Khodeir, *J. Am. Chem. Soc.* **2005**, *127*, 12028; b) A. Roy, S. Polarz, S. Rabe, B. Rellinghaus, H. Zähres, F. E. Kruis, M. Driess, *Chem. Eur. J.* **2004**, *10*, 1565.
[17] D. Schröder, H. Schwarz, S. Polarz, M. Driess, *Phys. Chem. Chem. Phys.* **2005**, *7*, 1049.
[18] V. Ischenko, S. Polarz, D. Grote, V. Stavarache, K. Fink, M. Driess, *Adv. Funct. Mater.* **2005**, *15*, 1945.
[19] S. Polarz, A. Roy, M. Merz, S. Halm, D. Schröder, L. Scheider, G. Bacher, F. E. Kruis, M. Driess, *Small* **2005**, *1*, 540.
[20] E. Lifshin, *X-Ray Characterization of Materials*, Wiley-VCH, Weinheim, **1999**.
[21] T. Genger, O. Hinrichsen, M. Muhler, *Catal. Lett.* **1999**, *59*, 137.

